JOURNAL OF SPACECRAFT AND ROCKETS
Vol. 29, No. 1, January-February 1992

Application of the LAURA Code for Slender-Vehicle Aerothermodynamics

Richard A. Thompson* and Peter A. Gnoffo†
NASA Langley Research Center, Hampton, Virginia 23665

Application of a three-dimensional thin-layer Navier-Stokes code (LAURA) to compute the laminar and turbulent perfect gas aerothermodynamics of slender vehicles is demonstrated in this paper. Comparison of solutions with experimental data enabled an assessment of the code's aerodynamic heating prediction capabilities. The results show radial grid refinement to a wall cell Reynolds number of 2 to be accurate for predicting aerodynamic heating to a slender cone. Additional comparisons for an 80-deg slab-delta wing, a generic aero-space plane vehicle, and an all-body configuration show the method to be generally accurate using this radial cell spacing. Discrepancies between the predicted and measured heating in a region of crossflow separation on the generic aero-space plane geometry are noted, which indicates the need for further study. Although additional applications and comparisons are required to fully test the LAURA program, the results of this study demonstrate the current level of confidence and the engineering utility of this particular code for slender-vehicle applications.

Nomenclature

a	= major axis of elliptical cross section
b	= minor axis of elliptical cross section
c	= speed of sound
L	= axial length
M	= Mach number
q	= heat transfer rate
q_{ref}	= reference heat transfer rate used for nondimensionalization
Re	= Reynolds number
Re_{cell}	= cell Reynolds number
r_n	= nose radius
s_o	= surface distance from leading edge of slab-delta wing
T	= temperature
U	= velocity
x	= axial distance
y	= spanwise distance
α	= angle of attack
Δn	= radial cell spacing at the wall
μ	= viscosity
ρ	= density

Subscripts

w	= value at the wall surface
∞	= value at freestream conditions

Introduction

INTEREST in a growing array of hypersonic vehicles in the past few years has prompted significant research in all design disciplines. One result of these efforts has been the development of new and refined computational tools for aerodynamic/aerothermodynamic analyses. However, with the development of new computer codes comes additional requirements in the evaluation, testing, and application of new techniques. Confidence in the predictive capability and an assessment of the engineering utility of these tools become of primary importance. A principal step toward this goal is the calculation and comparison of results with a range of experimental data. At this point, a practical knowledge of the accuracy and applicability of a computer code in an engineering environment is gained.

The purpose of the current paper is to demonstrate and evaluate the application of the LAURA (Langley Aerothermodynamic Upwind Relaxation Algorithm) code for aerothermodynamic analyses of slender hypersonic vehicles. As such, this study constitutes one step in the validation process. The LAURA code is a three-dimensional, finite volume, thin-layer Navier-Stokes solver developed by Gnoffo.[1-3] The primary development of this code for the past few years has been directed toward design requirements for the aeroassist flight experiment (AFE) vehicle and aeroassist space transfer vehicles (ASTV) in general. These vehicles are typically very blunt with large wake-flow regions. Since the LAURA code is completely general in terms of geometry, it can be applied to the other spectrum of shapes as well, namely, slender vehicles.

The direction of the present work was to use the LAURA code for aerothermodynamic predictions over more slender vehicles than those considered to date. In this respect, the study is directed toward the National Aero-Space Plane (NASP), which is receiving considerable attention within the hypersonic community. For the purposes of this paper, only laminar and turbulent perfect gas flow conditions were considered. A study of the LAURA code with real gas chemistry, and the associated effects on slender vehicle flowfields, would be the subject of another paper and is not included here. Nevertheless, the predictions presented herein are among the first aerothermodynamic results presented for slender three-dimensional vehicles using the LAURA code.

To evaluate the present results, the LAURA predictions are compared with various sources of ground-based experimental data. In this paper, we intend to contribute to the validation of the code for applications to slender three-dimensional configurations such as NASP by focusing on comparisons of surface heat transfer results. Previous studies concerning calibration of the LAURA code are reported in Refs. 4 and 5. The following sections of this paper give short descriptions of the prediction method and the experimental data used for comparison. This is followed by a discussion of the results and some conclusions related to the objectives of the paper. More complete

Presented as Paper 90-1714 at the AIAA/ASME 5th Joint Thermophysics and Heat Transfer Conference, Seattle, WA, June 18-20, 1990; received Feb. 25, 1991; revision received Aug. 21, 1991; accepted for publication Aug. 21, 1991.

*Aero-Space Technologist, Aerothermodynamics Branch, Space Systems Division. Senior Member AIAA.

†Aero-Space Technologist, Aerothermodynamics Branch, Space Systems Division. Associate Fellow AIAA.

details of the computational method and experimental data can be found in the references cited.

Computational Method

The code used in this paper (LAURA) was developed by Gnoffo[1-3] primarily to treat the blunt-body and wake flow around ASTV configurations. Gnoffo[6] has extended the original LAURA code to model finite rate chemistry and thermal nonequilibrium effects that are expected in the ASTV flight regimes. The majority of applications of the LAURA code to date have been for these very blunt vehicles. Some work with slender vehicles has been done by Greene,[7] wherein the global time relaxation of the LAURA code was replaced by spatial marching in the streamwise direction and time relaxation in the marching planes. Greene showed good agreement of his marching code with experimental heat transfer measurements to sphere cones and a shuttlelike geometry. In the present paper, the LAURA code is used in its original global time-relaxation form.

The LAURA code uses a finite volume approximation to the integral form of the thin-layer Navier-Stokes equations. A second-order-accurate symmetric total variation diminishing (STVD) scheme[8] is used in the upwinded differencing of the discretized equations. Roe's averaging[9] is employed to define variables at cell walls from the dependent variables at adjacent cell centers. The discretized equations are relaxed in time by global sweeps through the computational domain. In the relaxation scheme, dependent variables at a cell center are treated implicitly, whereas adjacent cell variables are treated explicitly using the latest available information in the iteration process. As a result, the relaxation only requires the inversion of a 5 × 5 matrix of the dependent variables at a cell center for the perfect gas case.

Grid adaption in the radial direction (away from the body surface) is performed during the relaxation sweeps. This adaption is used to move cells in and parallel to the shock layer once the bow shock is captured and also to cluster cells near the body surface for accurate boundary-layer and heat transfer calculations. Calculations are usually initiated with one-fourth of the desired number of radial cells and later enriched by successive doubling during the relaxation sweeps. This process promotes convergence and stability of the solution. The grid adaption procedure was enhanced in this study by incorporating the method of Nakahashi and Deiwert[10] to control the cell spacings away from the wall. At the wall, the cell Reynolds number, given by

$$Re_{\text{cell}} = \rho_w c_w \Delta n / \mu_w \tag{1}$$

was defined a priori and the resulting cell spacing then computed for every point on the body surface during the adaption process. No study of the refinement or adaption of cells in the axial or circumferential directions was performed.

Experimental Data

Sphere Cone

The spherically blunted cone is one of the simpler geometrical configurations to model; however, the flowfield surrounding a sphere cone can exhibit important features such as nose-bluntness effects and leeside vortices at angle of attack. Because of its simplicity, the sphere cone presents an easy candidate for code testing while providing some insight into flow phenomena associated with slender vehicles. Moreover, a wide range of experimental and computational results for sphere-cone vehicles exists in the literature for validation purposes.

One source of experimental data is the wind-tunnel tests performed by Cleary.[11] In these tests, heat transfer measurements were made for a 15-deg spherically blunted cone with two different nose radii at Mach 10.6 over a wide range of angle of attack. Thus, Cleary's data include effects due to variable nose bluntness and three-dimensional flow resulting from the angle-of-attack variation. These data have been used extensively in the past in comparisons with the full range of computational methods (approximate techniques to Navier-Stokes solvers). They are used in this paper to examine the effects of radial grid spacing on the LAURA code solutions as a precursor for the more geometrically complex vehicles that follow.

Slab-Delta Wing

The slab-delta wing is a good model for study since it incorporates some of the flow phenomena associated with NASP-like vehicles (e.g., flat windward surfaces with regions of inflow and outflow). In addition, an extensive experimental data base for both spherically blunted and sharp-prow slab-delta wings exists[12-14] at hypersonic flow conditions.

The 80-deg sweep slab-delta wing tested in Ref. 14 was considered in this paper. The experimental model in this case was approximately 14 nose radii long, as shown in Fig. 1. Thermocouple gauges were used to measure heating to the slab-delta wing along the windward centerline and in the crossplane. These crossplane measurements provide heating distributions from the leeside of the leading edge to the windward centerline in the direction perpendicular to the leading edge (Fig. 1). Because of the relatively short length of the model, the flow over the slab-delta wing was dominated by nose bluntness effects. Nevertheless, an important characteristic in the

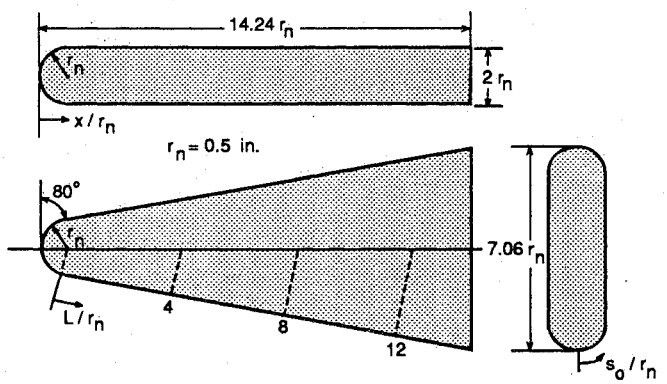

Fig. 1 Slab delta-wing geometry.

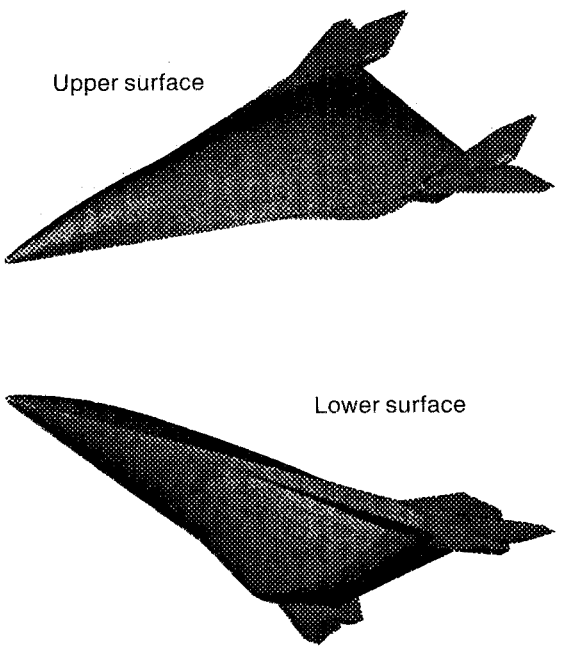

Fig. 2 Blended wing-body configuration.

flowfield (i.e., inflow on the windward side) was still evident in the experimental and computational results.

Blended Wing Body (National Aero-Space Plane Generic Option 2)

Moving in complexity from the sphere cone and slab-delta wing, the blended wing body (BWB) is a three-dimensional vehicle that includes nose bluntness, a flattened windward surface, leading-edge chines, and a double compression ramp system (Fig. 2). This generic configuration was one of several aerothermal, pressure, and force models tested in a series of studies[15] designed to investigate NASP technology and provide data for computational fluid dynamic (CFD) code validation. The BWB heat transfer and pressure model was tested experimentally in the Calspan shock tunnel[16] for Mach numbers ranging from 11.6 to 19.53 with Reynolds numbers from 0.11×10^6 to 11×10^6 per foot. Both sharp and blunted nose shapes were configured on the BWB and tests were run at angles of attack from 0 to 10 deg. Heat transfer measurements were made at over 100 surface locations and yielded distributions along the upper (leeward) and lower (windward) symmetry planes, along off-centerline rays on the lower surface, and in the crossplane direction. The extensive data base generated during these tests has been used for comparison[16-18] with several state-of-the-art computer codes. These experiments provide an excellent data set for code evaluation/verification and are used in the present paper for comparison with the LAURA results.

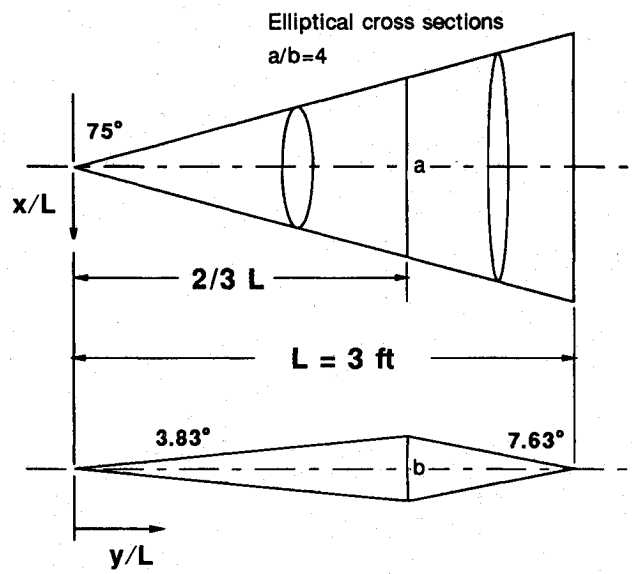

Fig. 3 NASA Ames all-body geometry.

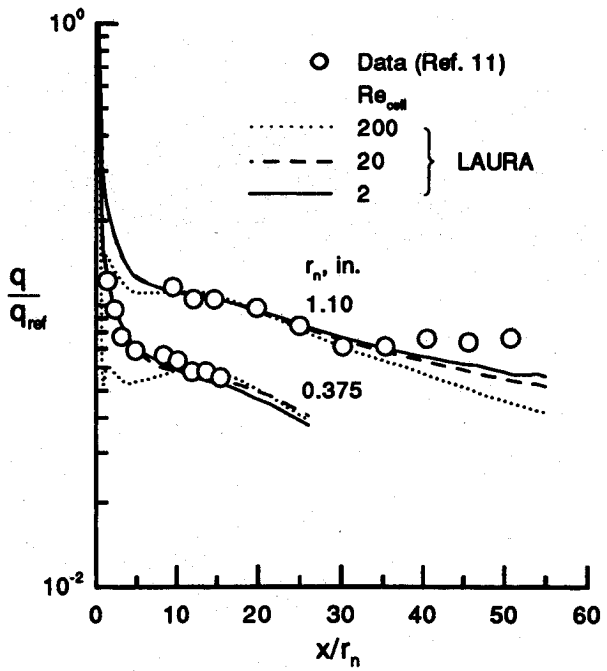

Fig. 4 Heat transfer results for the 15-deg sphere cone, $M_\infty = 10.6$.

NASA Ames All Body

The NASA Ames all-body investigation was designed to establish a benchmark experimental data base for a generic hypersonic vehicle that can be used for code validation/calibration.[19] The all-body model is representative of a hypersonic cruise vehicle with forward canards and combination vertical/horizontal tails. A test program was implemented to obtain surface and flowfield data for this configuration in the NASA Ames 3.5-ft Hypersonic Wind Tunnel over a range of conditions.

Test results for the all-body investigation have been published for a freestream Mach number of 7.4 at Reynolds numbers from 1.5×10^6 to 25×10^6 based on body length, and angles of attack from 0 to 15 deg. These conditions produce a broad range of phenomena including laminar to turbulent flows and attached to separated leeside flows. Data obtained on the all-body vehicle include shadowgraph and surface oil flow visualization studies, surface pressure and heat transfer measurements, and pitot probe flowfield surveys.

A sketch of the all-body geometry is shown in Fig. 3. The pressure and heat transfer models tested to date, depicted in this figure, do not include the carnards or tail surfaces. The sharp-tipped model has elliptical cross sections and is 3 ft in length. In the planform view, the body has a delta shape with a leading-edge sweep of 75 deg. As viewed from the side, the forebody has a 3.83-deg compression on the upper and lower surfaces followed by a 7.63-deg expansion surface to the end of the body. The compression surfaces produce a 4:1 elliptical cross section over the first two-thirds of the model length. The remaining length is characterized by increasingly elliptic cross sections that degenerate to a line at the trailing edge.

Results and Discussion

The comparison of predictions with experiment for each of the configurations considered are presented and discussed in this section. Note that the heating rates for every case are nondimensionalized by a reference value q_{ref} to mask the actual magnitudes. Both computational and experimental values are nondimensionalized by the same q_{ref} value for a given figure.

Sphere Cone

The sphere-cone geometry and test results from Cleary[11] were used initially to examine the effects of radial grid spacing on the LAURA code solutions. These heat transfer comparisons are shown in Fig. 4 for the 15-deg sphere cone fitted with two different nose radii (0.375 and 1.1 in.) at a 0-deg angle-of-attack condition. Freestream conditions for this case are presented in Table 1. Three radial spacings, corresponding to maximum cell Reynolds numbers Re_{cell} of 2, 20, and 200 at the body surface, were used for the LAURA predictions. A total of 64 cell volumes in the radial direction were used in each calculation with a constant grid stretching factor of 1.2 in this case. In the axial direction, 59 and 84 cells were used in the calculations for the large and small nose radius cones, respectively.

As seen in Fig. 4, the largest radial cell spacing (Re_{cell} = 200) results in a poor heat transfer prediction in comparison with the data for both nose radii bodies. Refining the spacing to Re_{cell} = 20 improves the prediction significantly, whereas further refinement has only a marginal effect. This last refinement (to Re_{cell} = 2) results in heating differences of less than 5% in comparison with the next coarser grid. Comparing the

Table 1 Freestream conditions

Geometry	M_∞	α, deg	U_∞, ft/s	ρ_∞, slug/ft^3	T_∞, °R	Re_∞, ft^{-1}
15-deg sphere cone	10.6	0.0	4795.7	1.89×10^{-5}	85.2	1.2×10^6
80-deg slab-delta wing	9.6	5.0	4348.9	2.01×10^{-5}	85.4	1.0×10^5
Blended wing body	12.4	6.0	7713.0	1.06×10^{-5}	161.2	5.7×10^5
NASA Ames all body	7.4	5.0	3816.0	1.21×10^{-4}	110.7	1.5×10^7

LAURA predictions for the fine radial spacing ($Re_{cell} = 2$) with the experimental data in Fig. 4 shows excellent agreement, except near the end of the large nose radius ($r_n = 1.1$ in.) body. The experimental heating in this region is higher than expected and may indicate a transitional state, which would account for the disagreement. Based on these results, a radial grid spacing with $Re_{cell} = 2$ at the body surface was chosen as a conservative value for the present heat transfer calculations and is used for all predictions in this paper.

Slab-Delta Wing

Comparisons of the LAURA predictions with experimental data for the 80-deg slab-delta wing are presented in Figs. 5 and 6. These results correspond to a case at Mach 9.6 and 5-deg angle of attack with the remaining freestream conditions shown in Table 1.

The geometry of the slab-delta wing is analytic so that modeling the body surface was straightforward. To discretize the flowfield around the slab-delta wing, 48 axial, 64 circumferential, and 64 radial cells were used. The radial cells were clustered at the body as discussed previously, whereas the circumferential cells were evenly spaced. In the axial direction, the cell walls were aligned along spherical coordinate rays in the nose region starting from an axis singularity and then in constant axial planes over the afterbody.

Measured and predicted heating distributions along the windward centerline of the slab-delta wing are compared in Fig. 5. Here, the prediction and data are in fair agreement, but the experimental data are underpredicted by 15–20%. Better agreement between prediction and experiment is shown in Fig. 6 for the crossplane heating distributions. This figure compares the distributions, in terms of surface distance measured from the wing leading edge ($s_o/r_n = 0$), for three streamwise stations (L/r_n). The experimental data extend from the leeside of the leading edge (negative s_o/r_n) around toward the windward centerline and are predicted generally well with the LAURA code. A region of crossflow separation on the leeside of the slab-delta wing was evident in the computed velocity profiles and is reflected by the increase in heating (Fig. 6) near the leeside symmetry plane. More important, the heating levels predicted for the separated region are comparable in magnitude with the heating to the windward surface. Unfortunately, there were no experimental data for comparison in this region.

Blended Wing Body

Two calculations for the blended wing body at an angle of attack of 6 deg were done corresponding to wind-tunnel conditions at Mach 12.4 and 16.7 and Reynolds numbers of 5.7×10^5 ft^{-1} and 1.1×10^5 ft^{-1}, respectively. Table 1 lists the other pertinent conditions for these cases. Only results from the case at Mach 12.4 are presented in this paper since the other calculations are similar and have been shown in Ref. 20. Initial and repeat runs were made at Calspan during the series of aerothermal tests for the Mach 12.4 condition. With the addition of spot heat transfer measurements during subsequent flow-survey runs, this case provides the most data on the BWB for a given flow condition. For clarity, only the data from two runs will be shown in the comparisons for this paper. Repeatability of the heat transfer measurements from the other runs was generally good. It should be noted that the wind-tunnel model was configured with a blunted nose tip in both cases, which was fully modeled and computed in the solutions. In addition, the present calculations only extend to the end of the compression ramp system ($x/L = 0.778$) and do not include the wing and vertical tail seen in Fig. 2.

In presenting the results for the BWB, the grid generation and other computational issues are discussed first, followed by

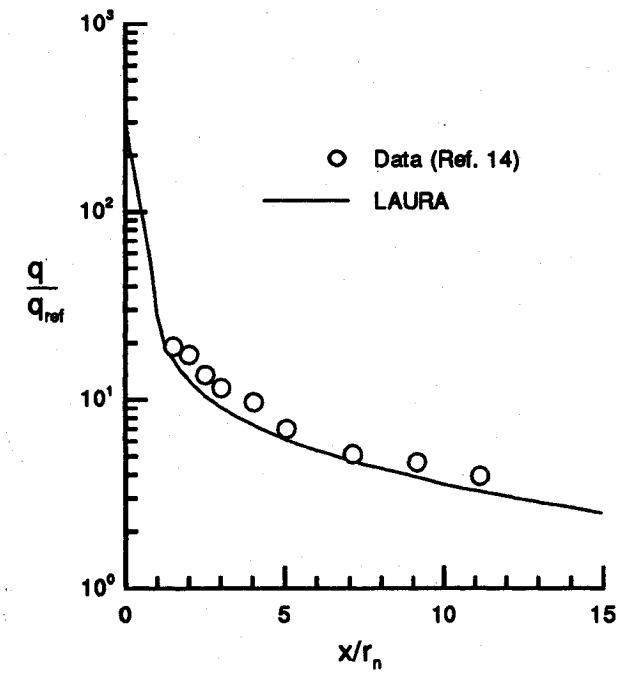

Fig. 5 Windward centerline heat transfer results for the slab-delta wing, $M_\infty = 9.6$.

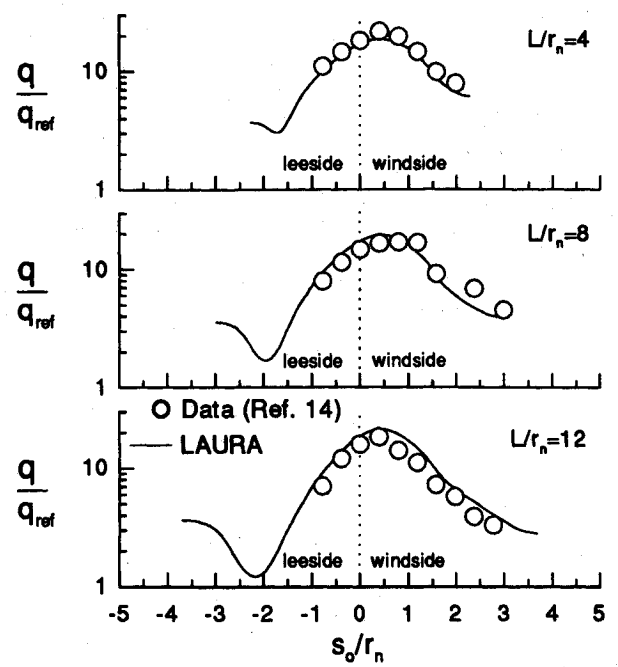

Fig. 6 Crossplane heat transfer results for the slab-delta wing, $M_\infty = 9.6$.

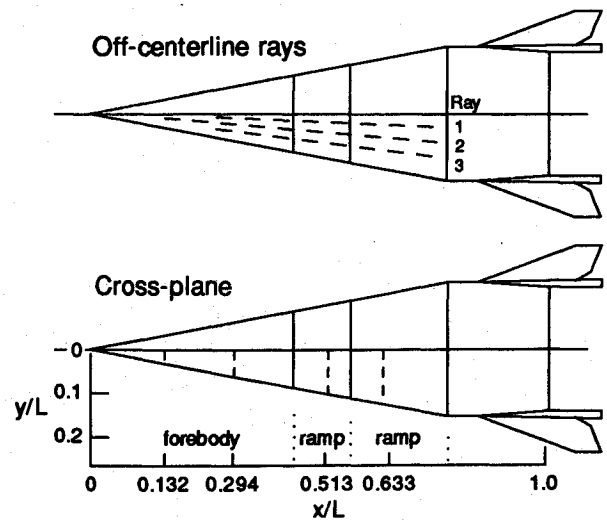

Fig. 7 Lower planform view of the blended wing body.

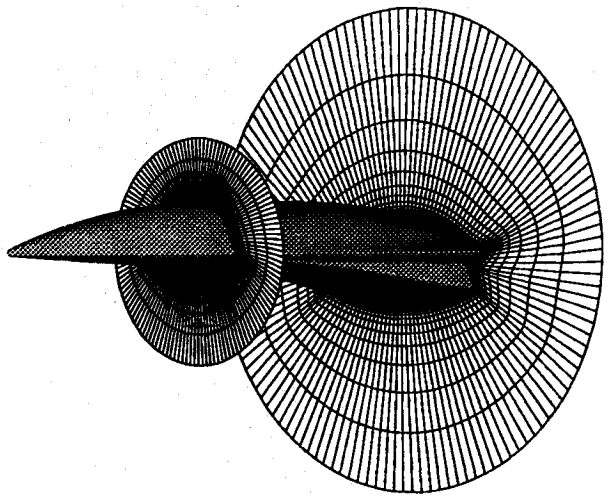

Fig. 8 Flowfield discretization for the blended wing body.

comparisons of the heating distributions in the symmetry plane, along off-centerline rays on the windward surface, and in the crossflow direction. Figure 7 shows the locations of these heat-transfer distributions in a planform view of the body surface.

Modeling the BWB required both an accurate surface definition and a flexible grid generation scheme. For these results, the surface of the vehicle was modeled using an interactive computer code[21] to fit the cross-sectional and longitudinal shape of the wind-tunnel model. This complete surface model provided the capability to generate body radii and flowfield grids at any cross section on the geometry.

A stacked two-dimensional grid approach was taken to discretize the three-dimensional flowfield over the forebody of the BWB. In this approach, two-dimensional grids were generated around cross sections of the BWB at specified axial locations. The three-dimensional grid is simply a collocation of these two-dimensional grids. An elliptic grid generation scheme was used to generate the two-dimensional grids, which provided some degree of grid orthogonality in the cross-sectional plane. The grid was clustered in the circumferential direction in each cross-sectional plane based on the local body curvature weighted with surface distance. This allowed the sharp corners and high-gradient regions to be modeled accurately while retaining a fair concentration of cells around the entire cross section. Grid generation for the blunted nose region of the BWB was handled somewhat differently than for the forebody. Here, the computational cells were constructed in a spherical coordinate system (with an axis singularity) that maintained the same circumferential grid clustering used on the forebody.

In the final arrangement, the physical domain was composed of 64 cells in the radial and circumferential directions and 41 cells in the streamwise direction. Radial clustering of cells was done such that the cell Reynolds number was equal to or less than 2 at every point on the body surface, as discussed previously. Also, the axial locations of the stacked two-dimensional grids were chosen to give somewhat finer grid resolution near the ramp junctures. Figure 8 shows the resulting cell distribution in two of the cross-sectional planes. For clarity, the grid shown is from the initial discretization before the radial adaption and enrichment of the solution procedure.

The comparisons of prediction with experiment for this case are presented in Figs. 9–12. Figure 9 shows the heat transfer predictions along the upper and lower symmetry planes in comparison with the measured data. The agreement between theory and experiment is excellent on the lower symmetry plane for the first 30% of the body and on the upper symmetry plane for the first 40%. Note that these regions are influenced by nose bluntness effects, which appear to be captured well in the numerical simulation. At the aft end of the upper (leeward) plane, the differences between prediction and experiment become larger with the predicted heating level under the measured values by 40% or more. These differences are believed to be caused by inadequate resolution of a region of crossflow separation. Finer grid spacing may improve the leeward comparison; however, no axial or circumferential grid refinement studies were performed for this paper. Such a study should be considered to resolve these differences. On the lower (windward) symmetry plane of the blended wing body (Fig. 9), the predicted heating level is 20–30% higher than was measured for the region beginning at about $x/L = 0.30$ and extending to the first ramp ($x/L = 0.433$). This overprediction may be due to underprediction of the strong inflow toward the centerline in this region. Downstream, the wide scatter in measured heating in the symmetry plane of the compression ramps indicates possible unsteady or transitional flow conditions.[16]

Although the comparison in Fig. 9 is generally poor on the aft windward centerline, the distributions of heating rates

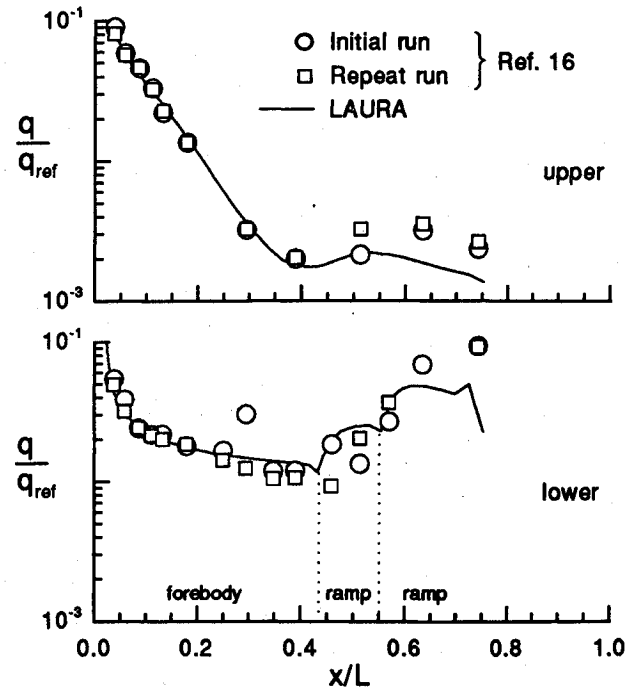

Fig. 9 Symmetry plane heat transfer results for the blended wing body, $M_\infty = 12.4$.

along off-centerline rays presented in Fig. 10 yield more information on the windward surface heating rates. The location of these rays on the lower surface with respect to the centerline are shown in Fig. 7. In contrast to the symmetry plane comparison, the agreement between experiment and prediction here is good to excellent on both of the compression ramps and for the area upstream of the first ramp. The good agreement along these windward surface rays and not along the symmetry plane indicates either some unknown phenomenon in the experimental results (e.g., transition or unsteadiness) or inadequate modeling in the computation. Considering the data scatter in the symmetry plane, it is not expected that the differences in the windward centerline comparisons can be resolved.

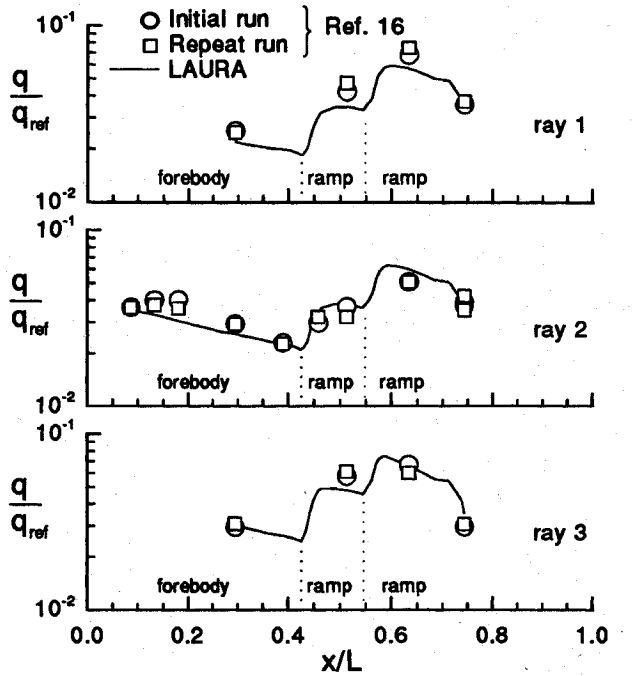

Fig. 10 Off-centerline heat transfer results for the blended wing body, $M_\infty = 12.4$.

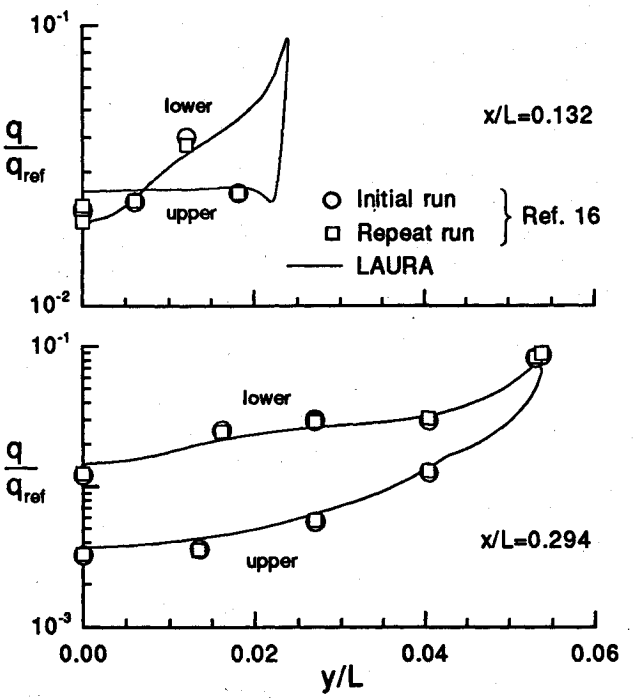

Fig. 11 Forebody crossplane heat transfer results for the blended wing body, $M_\infty = 12.4$.

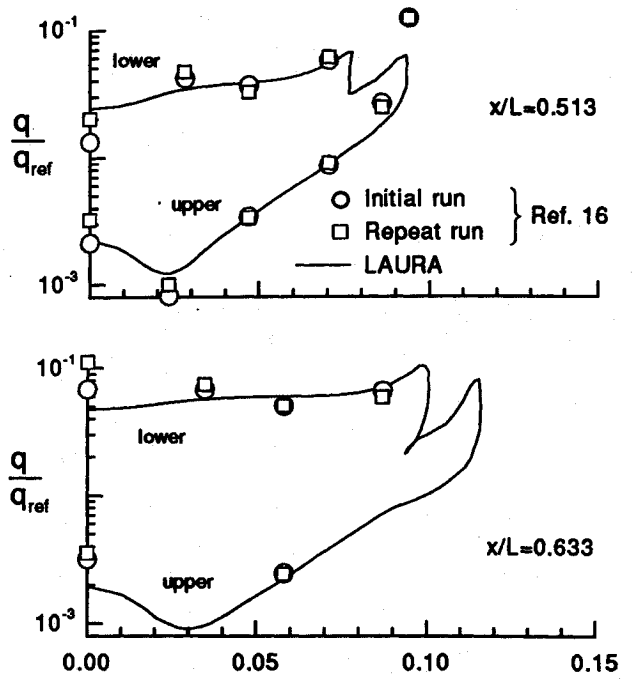

Fig. 12 Afterbody crossplane heat transfer results for the blended wing body, $M_\infty = 12.4$.

The remaining figures presented for this case (Figs. 11 and 12) show measured and computed heating distributions in the circumferential direction at four fuselage stations. These stations represent regions on the BWB forebody within the nose-dominated flowfield ($x/L = 0.132$), downstream of the nose effects ($x/L = 0.294$), on the first compression ramp ($x/L = 0.513$), and, finally, on the second ramp ($x/L = 0.633$). Figure 7 shows the locations of these stations in the planform view. The abscissa in these figures represents the buttline distance (y/L) measured from the plane of symmetry. Overall, the agreement between prediction and experiment is good and reflects the previous findings. That is, the predictions away from the symmetry plane ($y/L > 0.0$) are generally in better agreement with the experimental data. The repeatability of the experimental data shown in Figs. 11 and 12 is also good, in contrast to the windward centerline measurements. Note that the regions of high heating around the body corners and leading-edge chines are underpredicted (Fig. 12), presumably due to insufficient circumferential grid resolution. As mentioned previously, this may also be the cause for the poor agreement along the aft end of the upper centerline. In Fig. 12, the data and prediction both show a region of crossflow separation near the upper centerline; however, the discrepancies are difficult to assess from these heating results alone.

NASA Ames All Body

One test case condition at Mach 7.4, Reynolds number of 15 $\times 10^6$, and angle of attack of 5 deg was selected from the the middle range of the available data for the all-body configuration. Comparison of the measured and predicted heat transfer along the upper and lower plane of symmetry of the body is shown in Fig. 13 for this case. The LAURA prediction assumes turbulent flow over the vehicle and uses the algebraic eddy-viscosity model of Baldwin and Lomax[22] in the calculation. Transition was assumed to begin just downstream of the sharp nose as shown by the small peak in the predicted heating around $x/L = 0.01$. A region of nonlinear heating distribution is evident in the prediction on both the upper and lower symmetry plane for the first 20–25% of the length. This heating distribution was not seen in earlier predictions using a

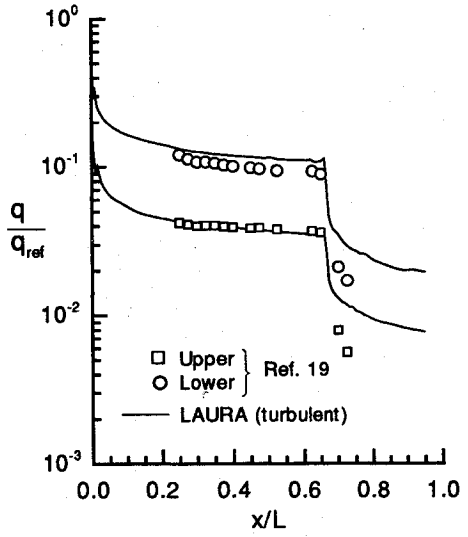

Fig. 13 Symmetry plane heat transfer results for the NASA Ames all body, $M_\infty = 7.4$.

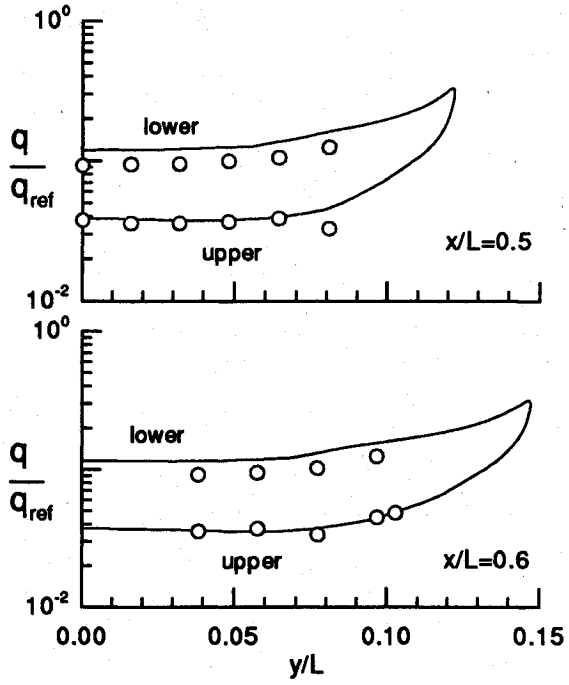

Fig. 14 Crossplane heat transfer results for the NASA Ames all body, $M_\infty = 7.4$.

parabolized Navier-Stokes code[19] and is thought to result from strong interaction effects in the sharp nose-tip region.

Comparing experiment with theory, the predicted heating is seen to be in excellent agreement on the forebody of the upper surface (before the expansion region) but 15–20% higher than measured on the lower surface. More striking is the poor agreement on both the upper and lower symmetry planes in the expansion region of the afterbody. Here, the predicted heating is roughly 50% higher than measured. Other published comparisons[19] with this data have shown similar disagreement in this region. However, comparisons (not shown here) of the computed and measured surface pressures are in excellent agreement in this region. In addition, a laminar calculation for this case showed that the measured heating was near midway between the predicted laminar and turbulent levels. It is probable that the disparity in heating is caused by some degree of relaminarization at the expansion corner, which is not modeled by the turbulent calculation. Similar reduction effects on turbulent heating have been shown[23] in experimental tests for an expansion biconic configuration.

The distribution of surface heat transfer in the crossplane direction on the all-body geometry is shown in Fig. 14. This figure compares the predicted heating rate with experimental measurements for axial stations at $x/L = 0.5$ and 0.6. The computed heating distributions on the lower surface are higher than measured but do exhibit similar trends moving from the centerline ($y/L = 0.0$) toward the peak heating at the leading edge. Measured and computed heating are in better agreement over the upper surface in these crossplane comparisons, similar to the results shown in the symmetry-plane comparisons. The axial variation of heating between the two crossplane stations is small for this angle-of-attack condition. Also note that a small local maximum in heating at the upper centerline is discernable in the computed results due to the reattachment of leeside vortices. Particle traces confirm the existence of this vortical flow in the computation, and oil flow studies have been reported[19] to show a similar result.

Conclusions

Application of a three-dimensional, thin-layer, Navier-Stokes code (LAURA) for slender-vehicle aerothermodynamics was demonstrated in this paper. Comparisons of predicted heat transfer with experimental measurements were made to assess the results. Perfect gas, laminar, and turbulent heat transfer cases were considered. A radial grid refinement study showed a wall cell Reynolds number of 2 to be accurate for predicting aerodynamic heating for a slender sphere cone. Calculations were performed for an 80-deg slab-delta wing at 5-deg angle of attack, a generic aero-space plane, and an all-body configuration. Comparisons with experimental data showed that the LAURA code could predict the heating generally well for these complex vehicles. Discrepancies in the predicted and measured heating in a crossflow-separated region of the aero-space plane geometry were noted, which indicated the need for further grid refinement and/or adaption studies. Although additional applications and comparisons are needed to fully test the LAURA code, the results of this study demonstrate the current level of confidence and the engineering utility of this particular code for slender-vehicle applications.

References

[1]Gnoffo, P. A., "Application of Program LAURA to Three-Dimensional AOTV Flowfields," AIAA Paper 86-0565, Jan. 1986.

[2]Gnoffo, P. A., McCandless, R. S., and Yee, H. C., "Enhancements to Program LAURA for Computation of Three-Dimensional Hypersonic Flow," AIAA Paper 87-0280, Jan. 1987.

[3]Gnoffo, P. A., "An Upwind-Biased, Point-Implicit Relaxation Algorithm for Viscous, Compressible Perfect-Gas Flows," NASA TP-2953, Feb. 1990.

[4]Gnoffo, P. A., "Code Calibration Program in Support of the Aeroassist Flight Experiment," *Journal of Spacecraft and Rockets,* Vol. 27, No. 2, 1990, pp. 131–142.

[5]Rudy, D. H., Thomas, J. L., Gnoffo, P. A., and Chakravarthy, S. R., "A Validation Study of Four Navier-Stokes Codes for High Speed Flow," AIAA Paper 89-1838, June 1989.

[6]Gnoffo, P. A., "Upwind-Biased Point-Implicit Relaxation Strategies for Viscous Hypersonic Flows," AIAA Paper 89-1972, June 1989.

[7]Greene, F. A., "An Upwind-Biased Space Marching Algorithm for Supersonic Viscous Flow," NASA TP-3068, March 1991.

[8]Yee, H. C., "On Symmetric and Upwind TVD Schemes," NASA TM-86842, Sept. 1985.

[9]Roe, P. L., "Approximate Riemann Solvers, Parameter Vectors, and Difference Schemes," *Journal of Computational Physics,* Vol. 43, No. 2, 1981, pp. 357–372.

[10]Nakahashi, K., and Deiwert, G. S., "Self-Adaptive-Grid Method with Application to Airfoil Flow," *AIAA Journal,* Vol. 24, No. 4, 1987, pp. 513–520.

[11]Cleary, J. W., "Effects of Angle of Attack and Bluntness on Laminar Heating-Rate Distributions of a 15° Cone at a Mach Number of 10.6," NASA TN D-5450, Oct. 1969.

[12]Whitehead, A. H., and Dunavant, J. C., "A Study of Pressure and Heat Transfer over an 80° Sweep Slab Delta Wing in Hypersonic

Flow," NASA TN D-2708, March 1965.

[13]Bertram, M. H., and Everhart, P. E., "An Experimental Study of the Pressure and Heat-Transfer Distribution on a 70° Sweep Slab Delta Wing in Hypersonic Flow," NASA TR R-153, Dec. 1963.

[14]Everhart, P. E., and Dunavant, J. C., "Heat-Transfer Distribution on 80° Slab Delta Wings at a Mach Number of 9.86 and Angles of Attack up to 90°," NASA TN D-2302, Oct. 1964.

[15]Anon., "Generic Technology Option #2—CFD Code Validation: Fourth Quarterly Review," McDonnell Douglas Corp., St. Louis, MO, Oct. 1987.

[16]Lau, K. Y., and Cosner, R. R., "Generic Technology Option #2—Final Report; Volume IV—Blended Wing-Body Aerothermal Model and Test Program," McDonnell Douglas Corp., St. Louis, MO, July 1988.

[17]Richardson, P. F., Parlette, E. B., Morrison, J., Switzer, G., and Dilley, D., "Heat Transfer and Pressure Comparisons Between Computation and Wind Tunnel for a Research Hypersonic Aircraft," AIAA Paper 89-0029, Jan. 1989.

[18]Krawczyk, W. J., "Analysis of Aerospace Vehicle Scramjet Propulsive Flow Fields: 3-D Forebody Code Development," NASP CR 1029, Nov. 1988.

[19]Lockman, W. K., Lawrence, S. L., and Cleary, J. W., "Experimental and Computational Surface and Flow-Field Results for an All-Body Hypersonic Aircraft," AIAA Paper 90-3067-CP, Aug. 1990.

[20]Thompson, R. A., and Gnoffo, P. A., "Application of the LAURA Code for Slender-Vehicle Aerothermodynamics," AIAA Paper 90-1714, June 1990.

[21]Cheatwood, F. M., and DeJarnette, F. R., "An Interactive User-Friendly Approach to Surface-Fitting Three-Dimensional Geometries," NASA CR-4126, March 1988.

[22]Baldwin, B. S., and Lomax, H., "Thin-Layer Approximation and Algebraic Model for Separated Turbulent Flows," AIAA Paper 78-257, Jan. 1978.

[23]Holden, M. S., "Experimental Studies of Surface Roughness, Entropy Swallowing and Boundary Layer Transition Effects on the Skin Friction and Heat Transfer Distribution in High Speed Flows," AIAA Paper 82-0034, Jan. 1982.

Ernest V. Zoby
Associate Editor